ADVANCED FUNCTIONAL MATERIALS

www.afm-journal.de

Development of Vanadium-Coated Carbon Microspheres: Electrochemical Behavior as Electrodes for Supercapacitors

Abdelhakim Elmouwahidi, Esther Bailón-García, Agustín F. Pérez-Cadenas, Nerea Fernández-Sáez, and Francisco Carrasco-Marín*

Vanadium-coated carbon-xerogel microspheres are successfully prepared by a specific designed sol–gel method, and their supercapacitor behavior is tested in a two-electrode system. Nitrogen adsorption shows that these composite materials present a well-developed micro- and mesoporous texture, which depends on the vanadium content in the final composite. A high dispersion of vanadium oxide on the carbon microsphere surface is reached, being the vanadium particle size around 4.5 nm. Moreover, low vanadium oxidation states are stabilized by the carbon matrix in the composites. The complete electrochemical characterization of the composites is carried out using cyclic voltammetry, chronopotentiometry, cycling charge–discharge, and impedance spectroscopy. The results show that these composites present high capacitance as 224 F g^{-1}, with a high capacitance retention which is explained on the basis of the presence of vanadium oxide, texture, and chemistry surface.

1. Introduction

Recently, with the increase of power and energy demands in various applications such as hybrid vehicles, large memory backup devices, and renewable-energy power plants, many efforts have been made to develop alternatives and more efficient energy storage devices. Electrochemical capacitors (also called supercapacitors) are investigated because of their unique characteristics such as fast charging–discharging, high power density, and long cycle lifetime.[1–3]

The selection of the material used as an electrode for a supercapacitor is crucial due to the porous structure and surface chemistry of the material, they are the key factors to the development of a supercapacitor with improved electrochemical performance including power density, energy density, rate capability, charging time, and cyclic stability. Generally, the charge storage in electrochemical capacitors occurs by a non-Faradaic process and a Faradaic/redox process. Typically, high surface area carbon-based materials reflect a non-Faradaic behavior (also known as electrochemical double-layer capacitors) whereas conductive polymers and metal oxides/hydroxides/sulfides have been desired as Faradaic process or pseudocapacitors associated with multiple oxidation states/structures that enable rich redox reactions for a pseudocapacitance generation.

Carbon materials have a high specific surface area,[1] high electronic conductivity, and an excellent stability. Therefore, activated carbons,[3,4] carbon fibers,[5–7] carbon aerogels,[8,9] and carbon spheres[10,11] have been commonly used as supercapacitor electrodes. However, these carbon-based electrochemical double-layer capacitors have a low capacitance, especially at high charge/discharge rates and low energy density and limited ionic accessibility.[2] Metal oxides and hydroxides overcome these limitations of carbon and usually exhibit a high specific capacitance, high power and energy densities.[3] Many metal oxides such as RuO_2,[12,13] ZnO,[14] MnO_2,[15,16] NiO,[17,18] Fe_2O_3,[19] and vanadium oxides,[20] especially V_2O_5, VO_2, and their hydroxides have been used for supercapacitors with good results, however, a decrease of their capacitances is observed by increasing the scan rate due to their lower conductivity.[21] Among the various metal oxides, vanadium pentoxide (V_2O_5) is considered to be one of the most promising candidates due to its wide potential window, unique layered structure, and a variety of oxidation states (V^{2+}, V^{3+}, V^{4+}, and V^{5+}) which can provide an excellent pseudocapacitance. However, the poor electrical conductivity, low specific capacitance, poor cycling stability, and low energy of the vanadium-based devices limit its real application. To overcome these limitations, the research is focused in three directions: i) preparing micro-/nanostructure materials, ii) the development of vanadium-based composite materials, and iii) the development of asymmetric supercapacitors.[22] The first approach leads to materials with a good surface area, high electrical conductivity, and a good cycling stability. But the synthesis method to prepare these materials is too complicated, expensive, and a low amount of material is obtained during the synthesis, avoiding a real industrial implantation. The development of composite materials is an interesting way to improve the electrical conductivity and the stability of the vanadium-based compounds. Nowadays, the preparation of vanadium-based materials and an electric double-layer capacitor (activated carbon, carbon nanotubes, graphene, etc.) has

---

Dr. A. Elmouwahidi, Dr. E. Bailón-García, Prof. A. F. Pérez-Cadenas,
N. Fernández-Sáez, Prof. F. Carrasco-Marín
Carbon Materials Research Group
Department of Inorganic Chemistry
Faculty of Sciences
University of Granada
Avenida de Fuentenueva, s/n, ES18071, Granada, Spain
E-mail: estherbg@ugr.es

The ORCID identification number(s) for the author(s) of this article can be found under https://doi.org/10.1002/adfm.201802337.

DOI: 10.1002/adfm.201802337

become a very hot research area. The idea of this approach is to get materials with an enhanced supercapacitor performance by combining advantages of both pure phases (surface area, conductivity, and stability of carbon materials and high power and energy density of metal oxides).

In previous works, Ti– and Zr–carbon xerogel composites have been synthesized and tested as electrodes for supercapacitors, obtaining an improved electrochemical performance with a high capacitance, a high retention capacitance, and a high energy density.[23,24] This improved behavior could be related to different properties of the composites: i) the presence of TiO_2 improves the hydrophilicity of the carbon surface which significantly increases the electrolyte contact with the surface, favoring the diffusion of the ions, ii) carbon matrix favors the TiO_2 reduction and these reduced species Ti^{3+} can act as electron transfer centers, decreasing the resistance of the electrode, iii) pseudo-Faradaic contributions of the TiO_2 phase, and iv) the presence of TiO_2 on carbon material induces a decrease in the resistance of the electrode, improving their performance for energy storage due to an optimization of the pore structure. A sample with a combination of low hydrophobicity and an adequate micro-mesopore network with a medium content in TiO_2 shows the best performance for the energy storage. In that sense, taking into account the benefits observed for Ti– and Zr–carbon xerogel composites and considering the multivalent state of vanadium which can provide an excellent pseudocapacitance, vanadium–carbon xerogel composites are presented as promising material in electrochemical devices.

On the other hand, the morphology of the material is also a quite important factor to consider during the preparation of supercapacitors. The use of carbon spheres shows many great advantages such as the high packing density which is very important for increasing the specific energy. These materials also have an excellent dispersivity and fluidity, leading to high performances in electrode manufacturing.[25]

With the abovementioned background, the development of vanadium-coated carbon spheres should be very interesting for electrochemical applications. Consequently, in the present work, carbon-xerogel microspheres were successfully covered for the first time, by a different amount of vanadium oxide being these composites deeply characterized from a textural, chemical, and electrochemical points of view, with a special emphasis in the study of their applications as electrodes for the supercapacitors.

2. Results and Discussion

2.1. Textural and Chemical Characterizations

2.1.1. Morphology and Dispersion

Scanning electron microscopy (SEM) and transmission electron microscopy (TEM) images of carbon spheres (CS) and vanadium oxide (VO)-coated carbon spheres (CSVX) are shown in **Figure 1**. As designed in an experimental setup, isolated microspheres of around 20 µm are obtained using the pregelled resorcinol-formaldehyde (RF) solution. The CS sample (Figure 1a,d) presents a clean and smooth surface, while the vanadium particles are clearly identified on the carbon sphere surface in the CSVX samples, increasing in number when the amount of theoretical vanadium increases from 5% to 18% (Figure 1b,c,e,f, respectively). VO-coated carbon microspheres show a high dispersion of vanadium oxide on the surface of carbon microspheres even at a high percentage of vanadium oxide. The presence of vanadium particles on the carbon surface was also corroborated by energy dispersive X-ray analysis (EDX) (Figure 1g–i). Vanadium is not detected in CS samples, whereas the signal of O and V increases on increasing the percentage of vanadium oxide in the final composite.

Dispersion and crystallinity of the vanadium oxide composites were analyzed by X-ray diffraction (XRD). XRD patterns of CSVX composites are shown in **Figure 2**a. Significant differences are observed between composites and pure V_2O_5. Four main diffractions peaks are obtained at values of 37.7°, 43.9°, 63.8°, and 76.6° for the CSVX composites which can be attributed to cubic V^{2+} (VO) (JCPDS 75-0048), while a more complex pattern is obtained for V_2O_5 attributed to orthorhombic phase (JCPDS 01-089-0612). Moreover, narrower and intense diffraction peaks were observed in V_2O_5, denoting a high crystallinity, while the diffraction peaks become wider and less intense in the case of CSVX composites. In that last case, the intensity of the peaks increases, increasing the amount of vanadium oxide. The mean average size of the vanadium oxide particles was estimated using the Debye–Scherrer equation, obtaining sizes of <4, 4.7, 4.8, 11.4, and 71.5 nm for CSV2, CSV5, CSV10, CSV18, and V_2O_5, respectively. This result denotes a good dispersion of VO nanoparticles on the carbon sphere surface. However, at quantities higher than 10%, this dispersion decreases but nevertheless, a very low crystal size is still obtained in comparison with pure vanadium oxide.

Note also that the vanadium oxidation state of the precursor is +5 and during the synthesis of C/V composites, a reduction of the vanadium occurs up to the most reduced state (+2), which is preserved after the cooling and the storage of the sample at room temperature. The valence of +5 is the most stable, while +4 and +2 are less stable and consequently, the mostly studied vanadium compounds in several application are VO_x (V_2O_5, V_2O_3, or even VO_2),[22] but a lack of information exists in the behavior of VO materials as supercapacitors. In that case, VO is mainly stabilized on vanadium-coated carbon spheres, which indicates that the carbon matrix favors in such a way this oxidation state stabilization.

2.1.2. Thermogravimetric Analysis (TGA)

The real amount of vanadium oxide in the final CSVX carbon composites was determined by the burning of the carbon phase by TGA. The final residual mass after TGA experiments was considered as the inorganic phase content. In this way, the real percentage of vanadium oxide on the carbonized composites was 2.95, 6.53, 14.04, and 23.11 wt% for CSV2, CSV5, CSV10, and CSV18, respectively. Comparing the TGA results with the theoretical ones, it is observed that the real percentages are slightly higher than the theoretical ones due to the weight loss undergone by the samples during carbonization is higher than 50%. Note also that this difference increases at a higher amount of vanadium oxide. Nevertheless, the similarity between the theoretical and real values points out an oxidation of VO to V_2O_5 during the TGA experiments. Also note that the presence of the vanadium oxide decreases the burn off temperature of

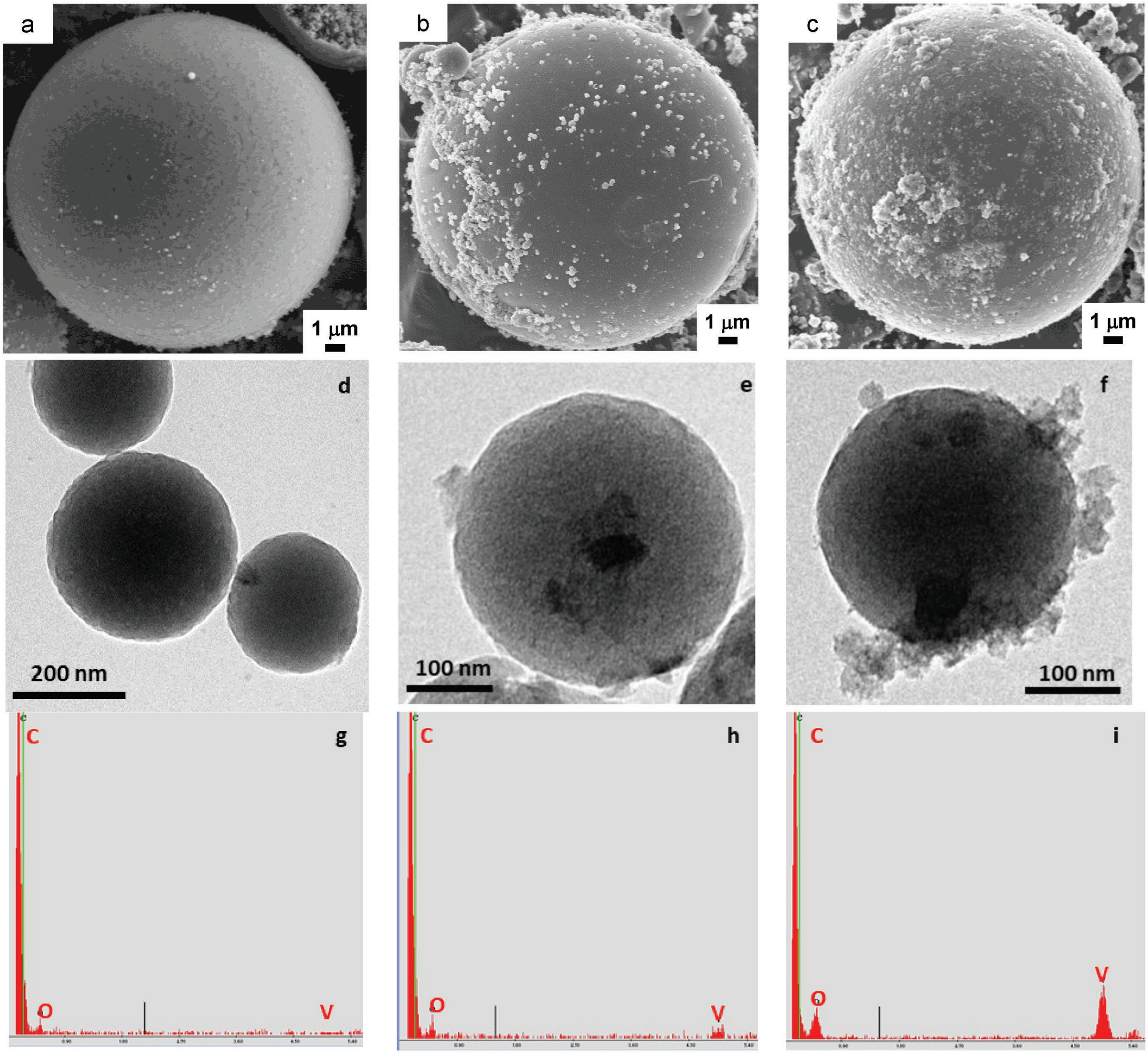

Figure 1. a–c) SEM, d–f) TEM, and g–i) EDX images of CS (a, d, g), CSV5 (b, e, h), and CSV18 (c, f, i).

the carbon matrix (around 300 °C) comparing to pure carbon spheres which start to burn at around 500 °C (Figure 2b). Moreover, an increase of weight is observed for composites at around 220 °C which could be ascribed to the V^{2+} oxidation. The vanadium oxide is a well-known oxidation catalyst with a high activity for the combustion of carbonaceous materials.[26–29] The catalytic activity of the vanadium catalysts for soot oxidation is correlated to their redox properties and the mobility of surface atoms. In particular, it has been suggested that the oxidation of soot involves a redox mechanism in which the catalyst is partially reduced by the extraction of oxygen from the catalyst which in turn is replaced by oxygen coming from gas phase.[29] The catalytic cycle is easily occurring because of the capability of the vanadium to easily change its oxidation state. This provides a high reactivity of the oxygen in the V=O bond, making favorable the oxygen needed for the oxidation of soot. On such a basis, the presence of VO on the surface of carbon spheres increases the capacity to store and release oxygen of vanadium oxide, increasing the ability to exchange oxygen with gas-phase O_2 and during this exchange process, highly reactive oxygen species are created which can be involved in different catalytic processes.[30] The highly reactive active oxygen atoms can oxidize carbon very efficiently, decreasing the combustion temperature.

2.1.3. N_2 and CO_2 Isotherm Adsorption

The pore structure of the samples was studied by N_2 and CO_2 adsorption measurements. The results are collected in

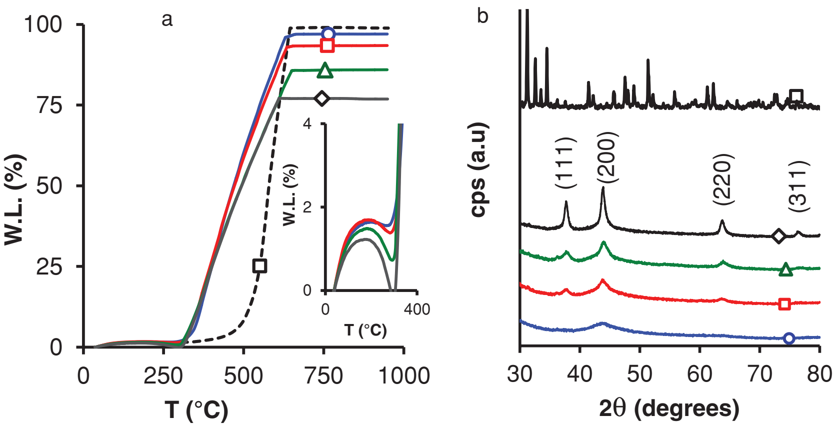

Figure 2. a) Powder XRD patterns and b) TGA profiles of CSVX composites and CS. CS (□, dashed line), V_2O_5 (□), CSV2 (○), CSV5 (□), CSV10 (△), and CSV18 (◇).

Table 1. All samples present Type I and IV hybrid isotherm characteristic of micro-, mesoporous solid. The content of vanadium oxide greatly affects the textural characteristics of the composites. The higher the percentage of vanadium oxide, the higher is the volume of the mesopores (V_{mes}) with a lineal relationship between both (Figure S1a, Supporting Information). The mesoporosity increases with the percentage of the vanadium oxide dispersed into the carbon xerogel surface and also the microporosity increases and becomes the widest ($W_0(N_2)$ and $L_0(N_2)$ increases, Figure S1b, Supporting Information) at the expense of the ultra-microporosity ($W_0(CO_2)$) that decreases (Figure 4). It is well-known that the CO_2 adsorption provides information about the narrow microporosity, corresponding to micropores with a diameter lower than 0.7 nm, while the total microporosity is obtained from N_2 isotherm only in the absence of diffusion restrictions. However, CO_2 is a polarizable molecule and thus, adsorption as well interaction CO_2–V are responsible for CO_2 uptake. Note that, increasing the amount of vanadium oxide, the CO_2 adsorption decreases despite the higher amount of vanadium sites which could improve their adsorption, manifesting that the CO_2 uptake by the CO_2–V interaction is minimum comparing with the CO_2 adsorption. In that sense, all samples show $W_0(N_2) < W_0(CO_2)$, but this difference becomes lower with the increase of the percentage of vanadium oxide due to the opening of the porosity observed, and thus, lower amount of ultra-micropores for CO_2 adsorption. Both micropores and mesopores are very important for their use as electrodes in energy storage applications because they have different roles with respect to a fast charge transfer and the double layer formation of electrolyte ions in the networks of the electrode.[7,31]

Considering the preparation method of these materials, carbon spheres covered by vanadium oxide, a blockage of porosity could be expected as it has been previously described.[32] A high decrease of microporosity was obtained when carbon spheres (CS) were covered by TiO_2 due to the microporosity blockage by TiO_2.[32] Conversely, new and wider porosity is created in the CSVX samples; higher at increasing the contents of vanadium. That could be explained on the basis of the ability of the vanadium oxide to catalyze oxidation reaction. V_2O_5 is obtained by hydrolysis of the vanadium isopropoxide as it is observed from XRD of organic gel. The low melting point of V_2O_5 (690 °C) provides a high mobility of the vanadium species during the carbonization, its Tammann temperature is around 230 °C.[33] The surface mobility of active species and the ability of vanadium species to provide a high reactive oxygen make favorable the oxygen needed for the oxidation reactions and consequently, produce a partial gasification of carbon spheres creating and opening the porosity ($W_0(N_2)$ and a V_{meso} increase at the expense of a narrower porosity, $W_0(CO_2)$). Because of this oxygen transfer as well as the thermal treatment, the reduced vanadium species are stabilized after the carbonization process. As commented above, higher differences between TGA and theoretical values of vanadium contents (V_xO_{yTG}/V_2O_5), Table 1, are obtained by increasing the amount of vanadium in the sample. This could be explained on the basis of a higher gasification of the carbon matrix during carbonization of organic gels, due to a higher amount of gasification catalyst (vanadium oxide). Density functional theory (DFT) plots are depicted in Figure S2 (Supporting Information). Narrow mesoporosity (3.0 nm) is observed in the CS sample, whereas a higher volume and wider mesopores (3.9 nm) are observed in CSV18 as a consequence of the above commented porosity opening/carbon gasification.

2.1.4. Surface Composition: X-Ray Photoelectron Spectroscopy (XPS) Analysis

Surface compositions of the samples were analyzed by XPS which provided information regarding the electronic states and

Table 1. Textural properties of the carbon–vanadium composites.

Sample	S_{BET} [$m^2\ g^{-1}$]	$W_0(N_2)$ [$cm^3\ g^{-1}$]	$W_0(CO_2)$ [$cm^3\ g^{-1}$]	$L_0(N_2)$ [nm]	$L_0(CO_2)$ [nm]	$V_{0,95}$ [$cm^3\ g^{-1}$]	V_{mes} [$cm^3\ g^{-1}$]	ρ[a)] [$g\ cm^{-3}$]	$VxOy_{TG}$ [%]	$VxOy_{TG}/V_2O_5$
CS	573	0.226	0.288	0.65	0.59	0.330	0.104	0.292	0	–
CSV2	568	0.225	0.282	0.70	0.60	0.336	0.111	0.467	2.95	1.15
CSV5	575	0.229	0.273	0.72	0.58	0.347	0.118	0.517	6.53	1.24
CSV10	602	0.241	0.266	0.75	0.60	0.356	0.115	0.560	14.04	1.26
CSV18	566	0.228	0.245	0.79	0.59	0.352	0.124	0.569	23.11	1.31

[a)] Bulk density.

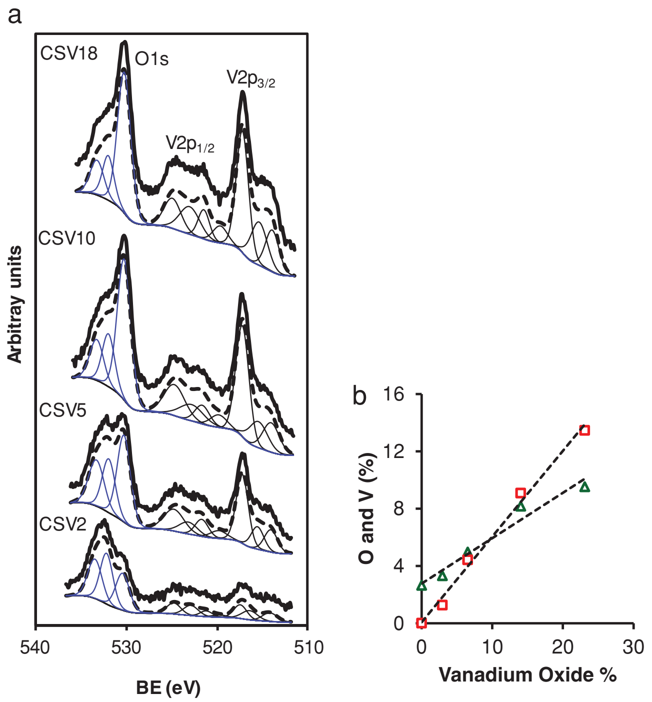

Figure 3. a) V_{2p} and O_{1s} spectral region, b) relation between surface V (□) and O (△) with percentage of vanadium oxide in the composite.

the chemical environment of carbon (C), vanadium (V), and oxygen (O) atoms in the composite materials. XPS data are collected in Table S1 (Supporting Information) and vanadium and oxygen regions are depicted in **Figure 3**. Six carbon components are needed to fix the C_{1s} spectral region in all cases; the main carbon peak is found at 284.6 eV, which corresponds to the nonoxygenated amorphous carbon. Peaks at 285.8, 286.8, and 288.1 eV are assigned to C—O, C=O, and COO^-, respectively. Note that there is no carbon peak associated with vanadium carbide (VC, binding energy (BE): 282.9 eV) in CSVX samples, suggesting that no carbothermal reduction took place during the synthesis. No significant differences between the C_{1s} region of pure carbon xerogel and CSVX composite are observed. In consequence, this fact can indicate that the presence of the vanadium oxide does not affect the surface chemistry of the carbon spheres.

Regarding the O_{1s} region, three different peaks were found: 530.3 eV is assigned to oxygen in a metal oxide,[34,35] whereas the peak located at 532 eV is characteristic either of a hydroxyl group (—OH) bonded or oxygenated groups like ketones (C=O) on the carbon surface.[36] The third component at 533.0 eV corresponds to acids, anhydrides, and lactones and also to ether groups (C—O—C).[36] Moreover, this assignation is confirmed by the fact that the first component increases progressively increasing the V-content in the composite, while the other ones slightly decrease due to the coverage of the carbon with vanadium species.

Three components are required to fit the $V_{2p3/2}$ region (Figure 3a); the peak at 513.9 eV corresponds to V^{2+} species, whereas the peaks at 515.5 and 517.1 eV are ascribed to V^{3+} and V^{4+} ones, respectively.[35,37] Analyzing the wt% of each element, as expected, a linear increase of percentage of V_{xps} and O_{xps} is obtained, increasing the vanadium oxide content on the carbon matrix (Figure 3b). From XRD analysis, only V^{2+} contribution would be expected on vanadium spectral region by XPS, however, a mixture of V^{2+}, V^{3+}, and V^{4+} oxidation states are obtained. Note that the more stable oxidation state, V^{5+}, is not detected. The presence of V^{3+} and V^{4+} components in the CSVX samples denotes an overoxidation at the surface of the sample from air exposure and since the technique is mostly sensitive to the first ≈10 nm beneath the surface, it is easily detected by the XPS measurements.

Silversmit et al.[38] concludes that the classical method to estimate the oxidation state in transition metal oxides based on the sensitivity factors may result in significant inaccuracies due to fact that the sensitivity factors for the 2p binding energies of transition metals largely vary because of the multielectron process dependency of the chemical state.[39] Alternatively, a mean oxidation state can be determined by computing the weighted percentage of the areas of the $V_{2p3/2}$ components. At this sense, a mean vanadium oxidation state can be determined from the ratio of the $V_{2p3/2}$ and O_{1s} XPS peak areas ($I(V_{2p3/2})$ and $I(O_{1s})$), when appropriate sensitivity factors, S, are known (Equation (1)).[38]

$$\text{Valence} = \frac{2\times I(O_{1s})/S(O_{1s})}{I\left(V_{2p_{3/2}}\right)/S\left(V_{2p_{3/2}}\right)} \tag{1}$$

The values used for the sensitivity factors $S(O_{1s})$ and $S(V_{2p3/2})$ are 0.66 and 1.3, respectively. A valence near to 3 is obtained in all cases, which really corroborates the stabilization of low vanadia valence on the carbon sphere surface.

2.2. Electrochemical Characterization of Vanadium–Carbon Composites

The electrochemical performances of the vanadium–carbon composites are measured using different electrochemical techniques such as cycling voltammetry (CV), electrochemical impedance spectroscopy (EIS), and galvanostatic charge/discharge using a 1 M H_2SO_4 as electrolyte.

Figure 4a depicts the cyclic voltammograms at a different scan rate for the sample CSV18. It is shown that the variation of the capacitance with the increase of the scan rate decreases the capacitance as the scan rate increases, because when the scan rate is high, the formation of the electrochemical double layer within the micropores is slower and less complete. As the scan rate increases, the current versus potential is deviated from the classical rectangular waveform, expected for a pure capacitor. As discussed by some researchers, this is due to the resistance effects inside the pores.[40] In addition to the pore resistance, efficiency is another important parameter affecting the capacitance in high sweep rates. As the sweep rate increases, the loss of energy increases and the stored charge on the electrode surface decreases, causing the capacitance decrease. Figure 4b shows the results of all samples at 5 mV s^{-1}. All carbon composites show a quasirectangular shape, typical voltammograms for electrochemical double-layer (EDL) capacitors with no diffusional restriction to the electrolyte[4,7] and furthermore, the cyclic voltammetry is effectuated in the

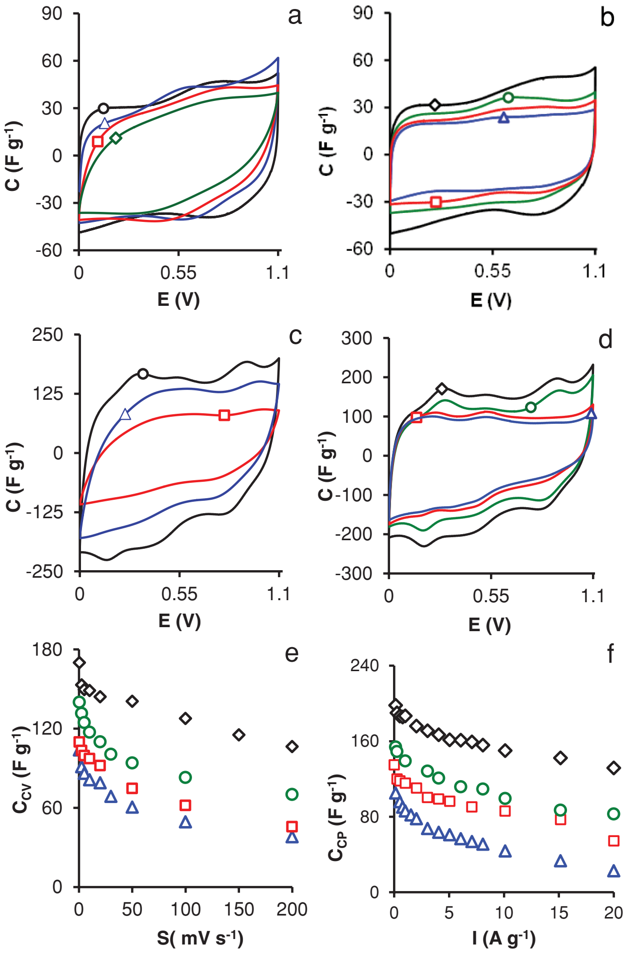

Figure 4. Cyclic voltammograms for sample CSV18 at different scan rates: 10 (○), 50 (△), 100 (□), and 200 (◇) mV s^{-1} in a) two-electrode and c) three-electrode system. Cyclic voltammograms at 5 mV s^{-1} for samples: CSV2 (△), CSV5 (□), CSV10 (○), and CSV18 (◇) in b) two-electrode and d) three-electrode system. Variation of the gravimetric capacitance against e) the scan rate, f) the current density for samples: CSV2 (△), CSV5 (□), CSV10 (○), and CSV18 (◇) in a two-electrode system.

voltage windows from 0 to 1.1 V, indicating a good stability of the electrodes due to the presence of the vanadium oxides in the composites. Moreover, it is important to highlight that despite of the two-electrode system used where Faradaic contribution is usually not observed, here a high contribution of Faradaic (redox) reactions could be easily identified related to the conversion between different vanadium oxidation states.[41] Faradaic contributions are not observed, for example, with similar TiO_2/C or ZrO_2/C composites when a two-system electrode is used, whereas they are observed in a three-system electrode.[23,24] This fact denotes the high ability of vanadium to provide excellent pseudocapacitance due to its multivalent character. In such a way, small heterogeneities in the electrodes provide a small asymmetry of the two-electrode system and due to the high Faradaic contribution of vanadium oxide, redox reactions are clearly observed.

To corroborate the possible pseudo-Faradaic contributions of vanadium oxide phase, cyclic voltammetry was performed on a three-electrode system using a Ag/AgCl electrode as the reference electrode. The results (Figure 4c,d) show that the presence of vanadium oxide produces load storage pseudo-Faradaic effects that are more important for composite with 18% of VO_x.

Chronopotentiograms (CPs) obtained are depicted in Figure S3 (Supporting Information) at a current load of a) 125 mA g^{-1} and b) 2 A g^{-1}. CPs show quasitriangular shapes which indicate again that samples behave as an ideal EDL performance with low resistance and a good diffusion of the electrolyte inside the pores.

The variation in the gravimetric capacitances measured by using both techniques (cyclic voltammetry (CV) and chronoamperometry, chronopotentiometry (CP)) are plotted in Figure 4c,d and compiled in **Table 2**. The pure carbon xerogel shows a lower capacitance due to its lower and narrower porosity and the absence of pseudo-Faradaic contributions. The C_{CP} values of the composites are very high, between 105 and 224 F g^{-1}, compared with the C100 sample. Volumetric capacitance values are also listed in Table 2 and range between 49 and 127 F cm^{-3}, with CSV18 showing the highest value. These values are much higher than the volumetric capacitance generally required for practical applications,[42,43] making these samples suitable for use in small-volume devices. Moreover, the higher the amount of vanadium oxide, the higher is the capacitance of the CSVX samples. This improvement in the capacitance can be related to the porous texture and the pseudo-Faradaic contributions of the vanadium oxide.

At this point, both contributions could be distinguished from the shape of the cyclic voltammograms and tried to be independently analyzed: i) a broad peak in the central region which is typical for Faradaic reactions of intercalating compounds and ii) a nearly rectangular background related to the electrochemical double-layer behavior and consequently mainly influenced by the porous structure and chemical properties. Considering the rectangular background, an area increase is observed, increasing the vanadium content. That improvement in capacitance could be explained by considering two parameters: pore size and pore volume. So, when the vanadium percentage increases from 2 to 18, the pore volume ($W_0(N_2)$) slightly decreased from 0.282 to 0.245 cm^3 g^{-1} but the pore diameter increases from 0.65 to 0.79 nm and the mesopore volume, V_{meso}, increases from 0.114 to 0.124 cm^3 g^{-1}. There are

Table 2. Electrochemical performances of V–C composites.

Sample	C_{CV} 0.5 mV s^{-1}		C_{CV} 200 mV s^{-1}		C_{CP} 0.125 A g^{-1}		C_{CP} 20 A g^{-1}		Ret. C_{CP}[a)]
	[F g^{-1}]	[F cm^{-3}]	[F g^{-1}]	[F cm^{-3}]	[F g^{-1}]	[F cm^{-3}]	[F g^{-1}]	[F cm^{-3}]	[%]
CS	40	12	–	–	37	11	3	1	8
CSV2	104	48	38	18	105	49	23	11	22
CSV5	110	57	39	20	135	70	54	28	40
CSV10	140	78	70	39	154	86	83	46	54
CSV18	170	97	106	61	224	127	132	75	59

[a)] Ret. C_{CP}: percentage of retention capacity by galvanostatic discharge at 20 A g^{-1} referred to 0.125 A g^{-1}.

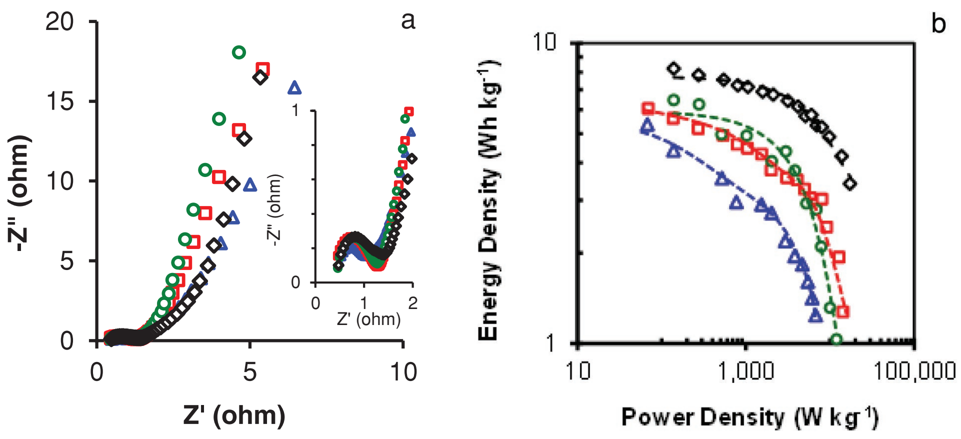

Figure 5. a) Nyquist and b) Ragone plots of samples: CSV2 (△), CSV5 (□), CSV10 (○), and CSV18 (◇).

many studies in literature suggesting that there is an increase of the specific capacitance with increasing the average pore size[44] due to the better accessibility of the electrolyte, in such a way, the creation and opening of the porosity observed in CSVX composites increasing the amount of vanadium oxide favors the electrolyte accessibility and consequently the capacitance. Related to the pseudo-Faradaic contributions, the higher the amount of vanadium oxide, the higher is the height of redox peak (Figure 4b) and consequently, the pseudo-Faradaic contributions. In this way, the opening of the microporosity together with the presence of more vanadium oxide, favors the supercapacitor behavior of the sample.

Another important factor to take into account in the design of supercapacitor materials is the capacitance retention at high current densities, which is a limiting factor to the use of carbon materials as electrodes. Figure 4f shows the variation of the specific capacitance, $C_{CP,}$ with the increase of the current density. C_{CP} decreases when the current load increases from 0.125 to 20 A g^{-1}, however, while CS present a very low capacity retention (8%), the presence of vanadium oxide increases the capacity retention of the samples. This increase in retention capacity is related with the increase in micropore width and mesopore volume which favors the transport of ions through the carbon porosity at a fast charge–discharge rate and so, facilitates the formation of the electrochemical double layer. CSV18 shows the highest capacitance retention (Table 2), 59%, because it has a higher mesopore volume than the other samples, which favors the transport of ions through the carbon porosity at a higher current density.

Figure 5a showed the EIS characterization of the CSVX composites. It shows the electrochemical impedance spectrum in the form of Nyquist plots, where Z' and Z'' are the real and imaginary parts of the impedance, respectively. In the high frequency region, the first intersection point on the real axis (Z') was the equivalent series resistance (ESR), which was related to the conductive properties of the activated carbon electrodes for comparison purposes, because the same electrolyte, collectors, and technique were used to assemble the cell.[45] The Nyquist plot contains a semicircle at medium to high frequencies, which is due to a Faradaic charge transfer resistance, R_{CT}, and a nearly straight line along the imaginary axis at a low-frequency component due to the mass transport limit. In the low frequency region, the imaginary part of the impedance (Z'') sharply increased and the plots tended to a vertical line, which is characteristic of the capacitive behavior. The maximum capacitance (C_{max}) of the composites was obtained at the lowest frequency (1 mHz), the results obtained are compiled in **Table 3**.

The difference of the R_{CT} for all the samples can be explained by the difference of the pore size diameter and Faradaic contributions which depends of the content of vanadium and carbon in the composite. The highest R_{CT} value was obtained for sample CSV18, which indicate that this is the sample where the pseudo-Faradaic effects are more important as is also depicted in Figure 4b,d. In general, all the sample composites show a lower ESR than CS, indicating a better penetration of the electrolyte into the pore structure.

The Ragone plots of the samples are shown in Figure 5b. This figure shows the dependence between the energy and power densities. The maximum energy density was released at the lowest power density (140 W kg^{-1}), as shown in Table 3.

The energy density of the CSVX composites is very high in comparison to the CS samples and there is a significant increase with the increase in vanadium content. A gradual decrease in energy density was observed when increasing the power density. The superior performance of sample CSV18 is due to its more developed porosity, with one of the highest values of mesopore volume in addition to the presence of vanadium. The higher energy density for CSV18 for both E_{max} and

Table 3. C_{max} at 1 mHz, equivalent series resistance (ESR), and charge transfer resistance (R_{CT}) from EIS and energy density at 140 W kg^{-1}, E_{max}, and at 7800 W kg^{-1}, E_{min}, (Wh kg^{-1}) from Ragone's plots.

Sample	ESR [Ω]	R_{CT} [Ω]	C_{max} [F g^{-1}]	E_{max} [Wh kg^{-1}]	E_{min} [Wh kg^{-1}]
CS	0.60	3.46	59	1.1	–
CSV2	0.49	0.62	96	4.4	0.9
CSV5	0.46	0.84	131	5.6	3.0
CSV10	0.46	0.85	155	6.5	2.8
CSV18	0.48	1.30	191	8.2	5.3

$E_{\min}$ should be highlighted, showing a retention of energy density of 69.8% in the potential range studied.

Cyclic stability of supercapacitors is one of the main factors for their practical applications. 13 000 galvanostatic charge–discharge cycles were applied over at a scan rate of 1 A g^{-1}, Figure S4 (Supporting Information). Results obtained indicate that the variation of specific capacitance of all the samples is very low, showing a capacitance retention of ≈98%.

3. Conclusions

Vanadium-coated carbon microspheres were, at the first time, prepared in a one-pot polymerization synthesis. A high dispersion of vanadium oxide on the surface of the carbon-xerogel microspheres was reached where the V^{2+} state is stabilized in these composites despite the fact that the stability of +4 and +2 oxidation states are less stable; therefore, carbon matrix clearly favors in such a way the stabilization of V^{2+} state. XPS shows the presence of the different reduction states of vanadium V^{2+}, V^{3+}, and V^{4+}, while V^{5+} was not detected ever. The presence of the V^{2+} state is also in agreement with the TGA results, since an increase of weight is observed for composites at around 220 °C. Moreover, the vanadium oxide content greatly affects the textural characteristics of the composites, in such a way that the higher the percentage of vanadium oxide, the higher the mesopore (V_{mes}) and micropore ($W_0(N_2)$) volumes, and micropores become wider at the expense of a decrease of the ultra-microporosity ($W_0(CO_2)$).

On the other hand, the electrochemical behavior of these materials is highly promising, since the sample CSV18 which corresponds to the composite with 18 wt% of vanadium oxide has a quite good specific capacitance, 224 F g^{-1} at current density of 125 mA g^{-1} in H_2SO_4, 1 M as electrolyte; furthermore, this sample was able to keep 58.8% of the capacitance at a high current density of 20 A g^{-1} and keep 100% of the capacitance over 13 000 charge–discharge cycles at 1 A g^{-1}. Moreover, this sample keeps the rectangular form of the voltammogram at a high scan rate of 200 mV s^{-1}, indicating a very good conductivity and stability of the electrode.

4. Experimental Section

Synthesis of Carbon–Vanadium Oxide Composites: Vanadium-coated carbon microspheres were prepared in a one-pot synthesis following a modified Pekala's polycondensation of resorcinol (R) with formaldehyde (F) in the presence of vanadium (V) tri-isopropoxide oxide as carbon and vanadium oxide precursors, respectively.[46] In a typical synthesis procedure, a pregelled (at 60 °C until the gel point) mixture of RF and water (W) was added dropwise to a *n*-heptane solution containing Span 80 (S) at 65 °C under refluxing and stirring (450 rpm). The molar ratio of the mixture was R/F = 1/2, R/W = 1/14, and R/S = 4.5. After 1 h, the proper amount of vanadium (V) tri-isopropoxide oxide 96% from Alfa Aesar was added dropwise to the reactor.

The formed gel was aged at 65 °C for 24 h under stirring and after that the suspension was filtered, the solid obtained was placed in acetone (5 days, changing acetone twice daily) to exchange water within the pores by acetone, in order to reduce the porosity collapse during the subsequent drying process and remove the Span 80. Then, the gel was dried by microwave heating using a Saivod MS-287W microwave oven under an argon atmosphere in periods of 1 min at 384 W until constant weight. Pyrolysis was carried out of organic xerogel–vanadium oxide composite to obtain the corresponding carbon xerogel–vanadium oxide composite in N_2 flow at 300 cm^3 min^{-1}, heating to 900 °C at a heating rate of 1 °C min^{-1}, in order to allow a soft removing of the pyrolysis gases, and a soaking time of 2 h. The amount of vanadium (V) tri-isopropoxide oxide needed to obtain 2.5%, 5%, 10%, and 18% of vanadium oxide on the final carbonized samples was calculated considering that V_2O_5 will be obtained after carbonization, a complete reaction between R and F and a weight loss of 50% during the carbonization. Samples were referred as CSVX (X corresponds to the theoretical percentage of vanadium oxide present in the carbonized composite, e.g., CSV10 means that carbon spheres were covered by 10 wt% of vanadium oxide. Also, a CS sample without vanadium oxide was prepared, following the same synthesis method and used as reference material.

Textural and Chemical Characterization: The morphology of the supports was studied by SEM using a LEO (Carl Zeiss) GEMINI-1530 microscope. The textural characterization was carried out by N_2 and CO_2 adsorption at −196 and 0 °C, respectively, using Quantachrome Autosorb-1 equipment. The Brunauer–Emmett–Teller (BET) and Dubinin–Radushkevich equations were applied to determine the apparent surface area (S_{BET}) and the micropore volume (W_0), the mean micropore width (L_0) and the microporous surface (S_{mic}), respectively. Furthermore, the DFT method was used to calculate the mesopore volume of the samples (V_{mes}). Pore size distributions were also obtained by applying the DFT method. The total pore volume was considered as the volume of N_2 adsorbed at $P/P_0 = 0.95$.

The vanadium oxide contents of the samples were determined by a TGA. The TGA was performed in flowing air with a heating rate of 10 °C min^{-1} using a Mettler-Toledo TGA/DSC1 thermogravimetric analyzer. The vanadium oxide phase was analyzed by a powder XRD pattern, using a Bruker D8 Advance X-ray diffractometer with Cu Kα radiation at a wavelength (λ) of 1.541 Å. The 2θ angles were scanned from 20° to 70°. The average crystallite sizes (D) were estimated by the Debye–Scherrer equation, $D = 0.95\lambda/\beta\cos\theta$, where θ is the diffraction angle and β is the full width at half-maximum (FWHM). The FWHM was determined with an extrapolated baseline between the beginning (low angle side) and the end (high-angle side) of a diffraction peak with the highest intensity.

The chemical characterization of the samples was further analyzed by XPS. The spectra were obtained on a Kratos Axis Ultra-DLD X-ray photoelectron spectrometer equipped with a hemispherical electron analyzer connected to a delay-line detector (DLD).

Electrochemical Characterization: For the electrochemical characterization, a mixture of active material and tetrafluoethylene (PTFE) binder (60% suspension in water) with a ratio of 90:10 was dried in an oven at 120 °C overnight. Then, 5 mg of the active material was pressed onto a graphite paper disk with 5 mm of diameter. The pasted sample was impregnated with a 1 M H_2SO_4 solution for 48 h before using it for the electrochemical measurements.

The electrochemical performances were determined using a two-electrode system with EC-lab equipment at 25 °C in H_2SO_4 1 M medium as electrolyte and glassy fibrous materials as a separator. Several electrochemical techniques were used for the electrochemical characterization of the composites. A cyclic voltammetry (CV) test was carried out within the range of 0–1.1 V; using scan rates from 0.5 to 200 mV s^{-1} and the galvanostatic charging–discharging was carried out at a different current densities from 125 mA g^{-1} to 20 A g^{-1}. The gravimetric capacitance from cyclic voltammetry tests, C_{CV} (F g^{-1}), and chronopotentiometric measurements, C_{CP} (F g^{-1}), was calculated following the methodology described elsewhere.[4,23] In order to analyze pseudo-Faradaic contributions of vanadia, a three-electrode system was also used to characterize the samples. For that, a typical three-electrode cell with Ag/AgCl as reference electrode, and Pt wire as counter electrode was employed.

The EIS measurements were carried out in the frequency of 100 kHz to 0.01 Hz. While, the stability of the electrodes was evaluated by charge–discharge cycles at a current density of 1 A g^{-1} between the potential value of 0 and 1.1 V over 13 500 charge–discharge cycles.

The electrical energy density and the power density were calculated by using the Equations (2) and (3), respectively, for two-electrode cell.[31,47]

$$E\,(\mathrm{Wh\,kg^{-1}}) = \frac{C_{\mathrm{GD}}(\mathrm{F g^{-1}}) \times (V_{\mathrm{max}}^2 - V_{\mathrm{min}}^2)\,(\mathrm{V})}{2 \times 3.6} \tag{2}$$

$$\mathrm{P}(\mathrm{W\,kg^{-1}}) = \frac{1}{2} \times \frac{I(\mathrm{A}) \times (V_{\mathrm{max}}^2 - V_{\mathrm{min}}^2)\,(\mathrm{V})}{m\,(\mathrm{kg})} \tag{3}$$

Supporting Information

Supporting Information is available from the Wiley Online Library or from the author.

Acknowledgements

This research was supported by the FEDER and Spanish projects CTQ2013-44789-R (MINECO) and P12-RNM-2892 (Junta de Andalucía). A.E. acknowledges a predoctoral fellowship from Erasmus Mundus, Al-Idrisi, programme. E.B.-G. is grateful to the MINECO for her postdoctoral fellowship, Juan de la Cierva programme.

Conflict of Interest

The authors declare no conflict of interest.

Keywords

carbon xerogels, electrochemical energy storage, electrodes for supercapacitors, vanadium-coated carbon microspheres

Received: April 5, 2018
Revised: June 8, 2018
Published online: July 5, 2018

[1] J. Chmiola, Y. Gogotsi, *Nanotechnol. Law Bus.* **2007**, *4*, 577.
[2] B. E. Conway, *Electrochemical Supercapacitors: Scientific Fundamentals and Technological Applications*, Springer Science+Business Media, New York **1999**.
[3] M. Sevilla, R. Mokaya, *Energy Environ. Sci.* **2014**, *7*, 1.
[4] A. Elmouwahidi, E. Bailón-García, A. F. Pérez-Cadenas, F. J. Maldonado-Hódar, F. Carrasco-Marín, *Electrochim. Acta* **2017**, *229*, 219.
[5] Q. Xie, R. Bao, C. Xie, A. Zheng, S. Wu, Y. Zhang, R. Zhang, P. Zhao, *J. Power Sources* **2016**, *317*, 133.
[6] C. Portet, G. Yushin, Y. Gogotsi, *Carbon* **2007**, *45*, 2511.
[7] T. Chen, L. Dai, *Mater. Today* **2013**, *16*, 272.
[8] Z. Zapata-Benabithe, F. Carrasco-Marín, C. Moreno-Castilla, *J. Power Sources* **2012**, *219*, 80.
[9] C. Moreno-Castilla, M. B. Dawidziuk, F. Carrasco-Marín, E. Morallón, *Carbon* **2012**, *50*, 3324.
[10] C. Moreno-Castilla, H. García-Rosero, F. Carrasco-Marín, *Colloids Surf., A* **2017**, *520*, 488.
[11] N. P. Wickramaratne, J. Xu, M. Wang, L. Zhu, L. Dai, M. Jaroniec, *Chem. Mater.* **2014**, *26*, 2820.
[12] J. P. Zheng, P. J. J. Cygan, T. R. R. Jow, *J. Electrochem. Soc.* **1995**, *142*, 2699.
[13] D. Rochefort, P. Dabo, D. Guay, P. M. A. Sherwood, *Electrochim. Acta* **2003**, *48*, 4245.
[14] X. Xiao, B. Han, G. Chen, L. Wang, Y. Wang, *Sci. Rep.* **2017**, *7*, 1.
[15] A. E. Fischer, K. A. Pettigrew, D. R. Rolison, R. M. Stroud, J. W. Long, *Nano Lett.* **2007**, *7*, 281.
[16] L. Wang, G. Duan, J. Zhu, S.-M. Chen, X. Liu, S. Palanisamy, *J. Colloid Interface Sci.* **2016**, *483*, 73.
[17] U. M. Patil, R. R. Salunkhe, K. V. Gurav, C. D. Lokhande, *Appl. Surf. Sci.* **2008**, *255*, 2603.
[18] H. Xiao, S. Yao, H. Liu, F. Qu, X. Zhang, X. Wu, *Prog. Nat. Sci.: Mater. Int.* **2016**, *26*, 271.
[19] G. S. Gund, D. P. Dubal, N. R. Chodankar, J. Y. Cho, P. Gomez-Romero, C. Park, C. D. Lokhande, *Sci. Rep.* **2015**, *5*, 1.
[20] J. M. Li, K. H. Chang, C. C. Hu, *Electrochem. Commun.* **2010**, *12*, 1800.
[21] Y. Wang, J. Guo, T. Wang, J. Shao, D. Wang, Y.-W. Yang, *Nanomaterials* **2015**, *5*, 1667.
[22] Y. Yan, B. Li, W. Guo, H. Pang, H. Xue, *J. Power Sources* **2016**, *329*, 148.
[23] A. Elmouwahidi, E. Bailón-García, J. Castelo-Quibén, A. F. Pérez-Cadenas, F. J. Maldonado-Hódar, F. Carrasco-Marín, *J. Mater. Chem. A* **2018**, *6*, 633.
[24] A. Elmouwahidi, E. Bailón-García, A. F. Pérez-Cadenas, F. J. Maldonado-Hódar, J. Castelo-Quibén, F. Carrasco-Marín, *Electrochim. Acta* **2018**, *259*, 803.
[25] H.-Q. Wang, Z.-S. Li, Y.-G. Huang, Q.-Y. Li, X.-Y. Wang, *J. Mater. Chem.* **2010**, *20*, 3883.
[26] D. W. McKee, *Carbon* **1970**, *8*, 623.
[27] G. Neri, G. Rizzo, S. Galvagno, M. G. Musolino, A. Donato, R. Pietropaolo, *Thermochim. Acta* **2002**, *381*, 165.
[28] D. Fino, N. Russo, G. Saracco, V. Specchia, *Top. Catal.* **2004**, *30–31*, 251.
[29] J. Liu, Z. Zhao, C. Xu, A. Duan, L. Zhu, X. Wang, *Appl. Catal., B* **2005**, *61*, 36.
[30] A. Bueno-López, *Appl. Catal., B* **2014**, *146*, 1.
[31] A. Bello, F. Barzegar, M. J. Madito, D. Y. Momodu, A. A. Khaleed, T. M. Masikhwa, J. K. Dangbegnon, N. Manyala, *Electrochim. Acta* **2016**, *213*, 107.
[32] E. Bailón-García, A. Elmouwahidi, M. A. Álvarez, F. Carrasco-Marín, A. F. Pérez-Cadenas, F. J. Maldonado-Hódar, *Appl. Catal., B* **2017**, *201*, 29.
[33] C. Moreno-Castilla, J. Rivera-Utrilla, A. J. López-Peinado, *Fuel* **1989**, *68*, 968.
[34] C. M. Ghimbeu, E. Raymundo-Piñero, P. Fioux, F. Béguin, C. Vix-Guterl, *J. Mater. Chem.* **2011**, *21*, 13268.
[35] M. C. Biesinger, L. W. M. Lau, A. R. Gerson, R. S. C. Smart, *Appl. Surf. Sci.* **2010**, *257*, 887.
[36] J. F. Vivo-Vilches, E. Bailón-García, A. F. Pérez-Cadenas, F. Carrasco-Marín, F. J. Maldonado-Hódar, *Carbon* **2014**, *68*, 520.
[37] A. Dey, M. K. Nayak, A. C. M. Esther, M. S. Pradeepkumar, D. Porwal, A. K. Gupta, P. Bera, H. C. Barshilia, A. K. Mukhopadhyay, A. K. Pandey, K. Khan, M. Bhattacharya, D. R. Kumar, N. Sridhara, A. K. Sharma, *Sci. Rep.* **2016**, *6*, 1.
[38] G. Silversmit, D. Depla, H. Poelman, G. B. Marin, R. De Gryse, *J. Electron Spectrosc. Relat. Phenom.* **2004**, *135*, 167.
[39] F. Ureña-Begara, A. Crunteanu, J. P. Raskin, *Appl. Surf. Sci.* **2017**, *403*, 717.
[40] B. E. Conway, W. G. Pell, *J. Power Sources* **2002**, *105*, 169.
[41] S. Boukhalfa, K. Evanoff, G. Yushin, *Energy Environ. Sci.* **2012**, *5*, 6872.
[42] W. Li, G. Reichenauer, J. Fricke, *Carbon* **2002**, *40*, 2955.
[43] Z. Zapata-Benabihe, C. Moreno-Castilla, F. Carrasco-Marín, *Langmuir* **2014**, *30*, 1716.
[44] F. Beck, M. Dolata, E. Grivei, N. Probst, *J. Appl. Electrochem.* **2001**, *31*, 845.
[45] D. Hulicova, M. Kodama, H. Hatori, *Chem. Mater.* **2006**, *18*, 2318.
[46] R. Pekala, D. Schaefer, *Macromolecules* **1993**, *26*, 5487.
[47] Y. Korenblit, M. Rose, E. Kockrick, L. Borchardt, A. Kvit, S. Kaskel, G. Yushin, *ACS Nano* **2010**, *4*, 1337.